Hot Nuclear Matter in Intense Magnetic Field

Kirill Tuchin

Department of Physics and Astronomy, Iowa State University, Ames, IA 50011

Abstract

Collision of two relativistic heavy ions produces highly intense electromagnetic field. Exact solution of Maxwell equations indicates that the field strength reaches $\sim m_\pi^2$ at RHIC and $\sim 10 m_\pi^2$ at LHC. Moreover, time-evolution of this field in electrically conducting nuclear matter is much slower than in vacuum. This fact has many important phenomenological consequences, two of which are discussed in detail: J/ψ dissociation in background magnetic field and synchrotron photon radiation by quark-gluon plasma.

Keywords: *Heavy-ion collisions; magnetic field; synchrotron radiation, J/ψ production*

1 Origin of magnetic field

Electromagnetic field of two relativistic heavy-ions can be estimated using elementary arguments. Suppose that each ion has radius R, electric charge Ze and collide at impact parameter $\boldsymbol{b}$. According to the Biot and Savart law they create magnetic field that in the center-of-mass frame has magnitude $B \sim \gamma Zeb/R^3$ and directed perpendicular to the collision plane, where $\gamma = \sqrt{s_{NN}}/2m_N$ is the Lorentz factor. At RHIC heavy-ions are collided at 200 GeV per nucleon, hence $\gamma = 100$. Using $Z = 79$ for Gold and $b \sim R_A \approx 7$ fm we estimate $eB \approx m_\pi^2 \sim 10^{18}$ G. To appreciate how strong is this field, compare it with the following numbers: the strongest magnetic field created on Earth in a form of electromagnetic shock wave is $\sim 10^7$ G, magnetic field of a neutron star is estimated to be $10^{10}-10^{13}$ G, that of a magnetar up to 10^{15} G.

It has been known for a long time that classical electrodynamics breaks down at the critical (Schwinger) field strength $F = m_e^2/e$. In cgs units the corresponding magnetic field is 10^{13} G. Because $m_\pi/m_e = 280$, electromagnetic fields created at RHIC and LHC are well above the critical value. This offers a unique opportunity to study the super-strong electromagnetic fields in laboratory. In the next section I present a classical solution to the problem of electromagnetic field in heavy-ion collisions. I then consider two phenomenological applications: Lorentz ionization of J/ψ in Section 3, and synchrotron photon radiation in Section 4.

2 Solution of Maxwell equations

In relativistic heavy-ion collisions, production of valence quarks in the central rapidity region – the baryon stopping – is suppressed. Hence Z valence quarks of each nucleus continue to travel after heavy-ion collision along the straight lines in opposite directions. These valence quarks carry total electric charge $2Ze$ that creates electromagnetic field in the interaction region. Unlike the valence quarks, gluons and sea quarks are produced mostly in the central rapidity region, i. e. in a plane perpendicular to the collision axis. It has been suggested by Landau long ago [1, 2] that

Proceedings of International Conference 'Nuclear Theory in the Supercomputing Era — 2013' (NTSE-2013), Ames, IA, USA, May 13–17, 2013. Eds. A. M. Shirokov and A. I. Mazur. Pacific National University, Khabarovsk, Russia, 2014, p. 175.

http://www.ntse-2013.khb.ru/Proc/Tuchin.pdf.

high multiplicity events in heavy-ion collisions can be effectively described using relativistic hydrodynamics. In particular, matter produced in heavy-ion collisions can be characterized by a few transport coefficients. This approach has enjoyed a remarkable phenomenological success (see, e. g., Ref. [3]). Since sea quarks carry electric charge, electromagnetic field created by valence quarks depends on the permittivity ϵ, permeability μ and conductivity σ of the produced matter.

Consider electromagnetic field created by a point charge e moving along the positive z-axis with velocity v. It is governed by Maxwell equations:

$$\boldsymbol{\nabla}\cdot\boldsymbol{B}=0, \qquad \boldsymbol{\nabla}\times\boldsymbol{E}=-\frac{\partial\boldsymbol{B}}{\partial t}, \tag{1}$$

$$\boldsymbol{\nabla}\cdot\boldsymbol{D}=e\,\delta(z-vt)\,\delta(\boldsymbol{b}), \qquad \boldsymbol{\nabla}\times\boldsymbol{H}=\frac{\partial\boldsymbol{D}}{\partial t}+\sigma\boldsymbol{E}+ev\hat{\boldsymbol{z}}\,\delta(z-vt)\,\delta(\boldsymbol{b}), \tag{2}$$

where $\boldsymbol{r}=z\hat{\boldsymbol{z}}+\boldsymbol{b}$ (such that $\boldsymbol{b}\cdot\hat{\boldsymbol{z}}=0$) is the position of the observation point. Introducing Fourier transforms of field components

$$\boldsymbol{E}(t,\boldsymbol{r})=\int_{-\infty}^{\infty}\frac{d\omega}{2\pi}\int_{-\infty}^{\infty}\frac{dk_z}{2\pi}\int\frac{d^2k_\perp}{(2\pi)^2}\,e^{-i\omega t+ik_zz+i\boldsymbol{k}_\perp\cdot\boldsymbol{b}}\,\boldsymbol{E}_{\omega\boldsymbol{k}}, \qquad \text{etc.,} \tag{3}$$

we can write the solution as follows:

$$\boldsymbol{H}_{\omega\boldsymbol{k}}=-2\pi iev\,\frac{\boldsymbol{k}\times\hat{\boldsymbol{z}}}{\omega^2\tilde{\epsilon}\mu-\boldsymbol{k}^2}\,\delta(\omega-k_zv), \quad \boldsymbol{E}_{\omega\boldsymbol{k}}=-2\pi ie\,\frac{\omega\mu v\hat{\boldsymbol{z}}-\boldsymbol{k}/\epsilon}{\omega^2\tilde{\epsilon}\mu-\boldsymbol{k}^2}\,\delta(\omega-k_zv), \tag{4}$$

where $\tilde{\epsilon}=\epsilon+i\sigma/\omega$ and ϵ, μ are functions of ω that depend on matter properties.

Later time dependence of electromagnetic field is determined by a singularity of Eq. (4) in the plane of complex ω that has smallest imaginary part. To obtain a conservative estimate of the matter effect we assume that the leading singularity is determined by electrical conductivity. Therefore, we adopt a simple model $\epsilon=\mu=1$, i. e. neglect polarization and magnetization response of nuclear matter, but take into account its finite electrical conductivity. Plugging (4) into Eq. (3) we take first trivial k_z-integral. Integration over ω for positive values of $x_-=t-z/v$ is done by closing the integration contour over the pole in the lower half-plane of complex ω. In the relativistic limit $\gamma=1/\sqrt{1-v^2}\gg1$ the result is [4,5]

$$\boldsymbol{H}(t,\boldsymbol{r})=H(t,\boldsymbol{r})\hat{\boldsymbol{\phi}}=\frac{e}{2\pi\sigma}\hat{\boldsymbol{\phi}}\int_0^\infty\frac{J_1(k_\perp b)\,k_\perp^2}{\sqrt{1+\frac{4k_\perp^2}{\gamma^2\sigma^2}}}\exp\left\{\frac{1}{2}\sigma\gamma^2x_-\left(1-\sqrt{1+\frac{4k_\perp^2}{\gamma^2\sigma^2}}\right)\right\}dk_\perp, \tag{5}$$

$$E_z(t,\boldsymbol{r})=\frac{e}{4\pi}\int k_\perp\,J_0(k_\perp b)\,\frac{1-\sqrt{1+\frac{4k_\perp^2}{\gamma^2\sigma^2}}}{\sqrt{1+\frac{4k_\perp^2}{\gamma^2\sigma^2}}}\exp\left\{\frac{1}{2}\sigma\gamma^2x_-\left(1-\sqrt{1+\frac{4k_\perp^2}{\gamma^2\sigma^2}}\right)\right\}dk_\perp, \tag{6}$$

$$\boldsymbol{E}_\perp(t,\boldsymbol{r})=H(t,\boldsymbol{r})\hat{\boldsymbol{r}}, \tag{7}$$

where $\hat{\boldsymbol{r}}$ and $\hat{\boldsymbol{\phi}}$ are unit vectors of polar coordinates in transverse plane x,y. Electromagnetic field is a function of $\boldsymbol{r}-\boldsymbol{r}'$, where $\boldsymbol{r}$ and $\boldsymbol{r}'=vt\hat{\boldsymbol{z}}$ are the positions of the observation point and the moving charge correspondingly. In fact, it depends only on distances $z-vt=-vx_-$ and b.

Equations (5)–(7) have two instructive limits depending on the value of parameter $\gamma\sigma b$ that appears in the exponents once we notice that $k_\perp\sim1/b$. If $\gamma\sigma b\ll1$, then, after a simple integration, Eqs. (5)–(7) reduce to the boosted Coulomb potential in free space:

$$\boldsymbol{E}=\frac{e\gamma}{4\pi}\frac{\boldsymbol{b}-vx_-\hat{\boldsymbol{z}}}{(b^2+\gamma^2v^2x_-^2)^{3/2}}, \qquad \boldsymbol{H}=\frac{e\gamma}{4\pi}\frac{v\hat{\boldsymbol{\phi}}}{(b^2+\gamma^2v^2x_-^2)^{3/2}}. \tag{8}$$

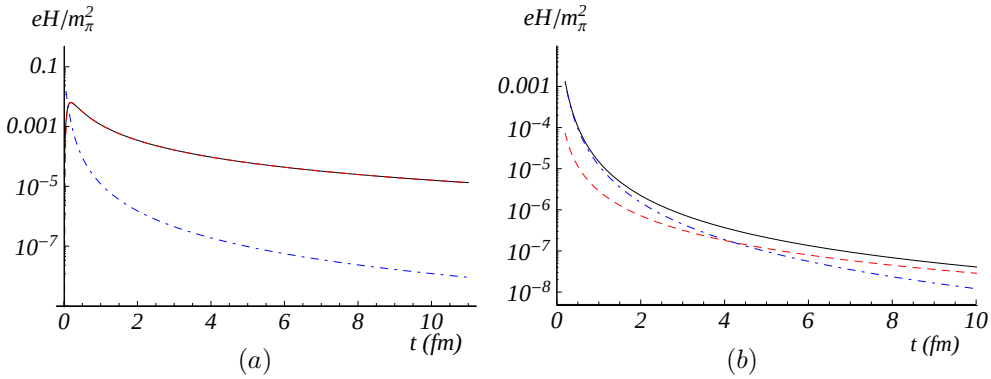

Figure 1: Time evolution of magnetic field created by a point unit charge at $z = 0$, $b = 7.4$ fm, $\gamma = 100$ and (a) $\sigma = 5.8$ MeV, (b) $\sigma = 0.01$ MeV. Black solid line is numerical computation of Eq. (5), red dashed line is "diffusion" approximation (9), blue dash-dotted line is a solution in free space.

This is the solution discussed in Ref. [6]. In the opposite limit $\gamma\sigma b \gg 1$, we expend the square root in Eqs. (5), (6) and derive

$$E_r = H_\phi = \frac{e}{2\pi}\frac{b\sigma}{4x_-^2}e^{-\frac{b^2\sigma}{4x_-}}, \qquad E_z = -\frac{e}{4\pi}\frac{x_- - b^2\sigma/4}{\gamma^2 x_-^3}e^{-\frac{b^2\sigma}{4x_-}}. \tag{9}$$

This is the solution suggested in Ref. [7]. Notice that the electromagnetic field in Eq. (8) drops as $1/x_-^3$ at late times, whereas in conducting matter only as $1/x_-^2$. At RHIC $\gamma = 100$, $\sigma \approx 5.8$ MeV [8–10]. For $b = 7$ fm we estimate $\gamma\sigma b = 19$, hence the field is given by the "diffusive" solution (9). This argument is augmented by numerical calculation presented in Fig. 1. In Fig. 1(a) we plot the result of numerical integration in Eq. (5) for $\sigma \approx 5.8$ MeV and compare it with the asymptotic solutions (8) and (9). It is seen that solution (9) completely overlaps with the exact solution at all times, except at $t < 0.1$ fm (not seen in the figure). To illustrate what happens at $\gamma\sigma b \ll 1$, we plotted in Fig. 1(b) the same formulas as in Fig. 1(a) calculated at artificially reduced conductivity $\sigma \approx 0.01$ MeV. One can clearly observe that at early time matter plays little role in the field time-evolution which follows Eq. (8), whereas at later time Foucault currents eventually slow down magnetic field decline, which then follows Eq. (9).

To obtain the total electromagnetic field of two colliding ions one needs to sum over all electric charges, which can be approximated by convolution (5)–(7) with nuclear densities. The resulting time dependence of total magnetic field is shown in Fig. 2.

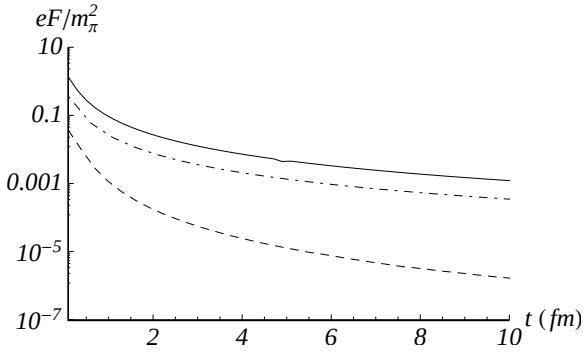

Figure 2: Time dependence of total electromagnetic magnetic field F at mid-rapidity $z = 0$, $\gamma = 100$, $B = 7$ fm, $t = 2$ fm. Solid line: $F = H_y$ at $x = y = 0$, dashed line $F = -H_x$ at $x = y = 1$ fm, dashed-dotted line $F = -E_y$ at $x = y = 1$ fm.

As expected late time dependence of all components is the same and governed by Eq. (9).

Transverse coordinate structure of electromagnetic field was investigated in Ref. [4] were it was observed that the space variation of H_y is mild. Other transverse components vary more significantly as they are required to vanish at either $x = 0$ or $y = 0$ by symmetry. When averaged over the transverse plane, only H_y component survives. In the following section we will consider phenomenological effect of constant magnetic field $\boldsymbol{B} = B\hat{\boldsymbol{y}} = H_y\hat{\boldsymbol{y}}$.

3 J/ψ in magnetic field

Strong magnetic field created in heavy-ion collisions generates a number of remarkable effects on quarkonium production.

1. *Lorentz ionization.* Consider quarkonium traveling with constant velocity in magnetic field in the laboratory frame. In quarkonium comoving frame, we find mutually orthogonal electric and magnetic fields given by Eqs. (10). In the presence of electric field quark and antiquark have a finite probability to tunnel through the potential barrier thereby causing quarkonium dissociation. We discuss this effect at length below.

2. *Zeeman effect.* Magnetic field lifts degeneration of quarkonium states with respect of the total angular momentum projection J_y. The corresponding splitting is of the order $\Delta M = \frac{eB_0}{2m} g J_y$, where $J_y = -J, -J+1, \dots, J$, m is quark mass and g is Landé factor. For example, J/ψ state with spin $S = 1$, orbital angular momentum $L = 0$ and total angular momentum $J = 1$ has $g \approx 2$ and splits into three states with $J_y = \pm 1, 0$ with mass difference $\Delta M = 0.15$ GeV at $eB_0 = 15 m_\pi^2$. Thus, the Zeeman effect leads to the emergence of new quarkonium states in plasma.

3. *Distortion of the quarkonium potential* in magnetic field. This effect arises in higher order perturbation theory and becomes important at field strengths of order $B \sim 3\pi m^2/e^3$ [11]. This is $3\pi/\alpha$ times stronger than the critical Schwinger's field. Therefore, this effect can be neglected at the present collider energies.

In this section I focus on Lorentz ionization, which contributes to J/ψ suppression in heavy-ion collisions [12, 13]. Before we proceed to analytical calculations it is worthwhile to discuss the physics picture in more detail in two reference frames: the quarkonium proper frame and the lab frame. In the quarkonium proper frame the potential energy of, say, antiquark (with $e < 0$) is a sum of its potential energy in the binding potential and its energy in the electric field $-eEx$, where x is the electric field direction. Since $|e|Ex$ becomes large and negative at large and negative x (far away from the bound state) and because the quarkonium potential has finite radius, this region opens up for the motion of the antiquark. Thus there is finite quantum mechanical probability to tunnel through the potential barrier formed on one side by the vanishing quarkonium potential and on the other by increasing absolute value of the antiquark energy in electric field. Of course, the total energy of antiquark (not counting its mass) is negative after tunneling. However, its kinetic energy grows proportionally to eEx as it goes away. By picking up a light quark out of vacuum it can hadronize into a D-meson.

If we now go to the reference frame where $E = 0$ and there is only magnetic field B (we can always do so since $E < B$), then the entire process looks quite different. An energetic quarkonium travels in external magnetic field and decays into quark-antiquark pair that can late hadronize into D-mesons. This happens in spite

of the fact that J/ψ mass is smaller than masses of two D-mesons due to additional momentum $e\boldsymbol{A}$ supplied by the magnetic field. Similarly, a single photon can decay into electron-positron pair in external magnetic field.

Consider a J/ψ traveling with velocity $\boldsymbol{V}$ in constant magnetic field $\boldsymbol{B}_0$ (subscript 0 indicates the laboratory frame). Let $\boldsymbol{B}$ and $\boldsymbol{E}$ be magnetic and electric fields in the comoving frame, and let subscripts $\parallel$ and $\perp$ denote field components parallel and perpendicular to $\boldsymbol{V}$ correspondingly. Then,

$$E_\parallel = 0, \qquad \boldsymbol{E}_\perp = \gamma_L \boldsymbol{V} \times \boldsymbol{B}_0, \tag{10a}$$

$$B_\parallel = \frac{\boldsymbol{B}_0 \cdot \boldsymbol{V}}{V}, \qquad \boldsymbol{B}_\perp = \gamma_L \frac{(\boldsymbol{V} \times \boldsymbol{B}_0) \times \boldsymbol{V}}{V^2}, \tag{10b}$$

where $\gamma_L = (1 - V^2)^{-1/2}$. Clearly, in the comoving frame $\boldsymbol{B} \cdot \boldsymbol{E} = 0$. We choose y and x axes of the comoving frame such that $\boldsymbol{B} = B\hat{\boldsymbol{y}}$ and $\boldsymbol{E} = E\hat{\boldsymbol{x}}$. A convenient gauge choice is $\boldsymbol{A} = -Bx\,\hat{\boldsymbol{z}}$ and $\varphi = -Ex$. The relative strength of electric and magnetic fields in comoving frame is $\rho = E/B$. This parameter is always in the range $0 \le \rho \le 1$ because $B^2 - E^2 = B_0^2 \ge 0$. When J/ψ moves perpendicularly to the magnetic field $\boldsymbol{B}_0$, $\rho = V$.

The force binding q and $\bar{q}$ in J/ψ is short-range in the sense that $(M\varepsilon_b)^{1/2} R \ll 1$, where ε_b and M are binding energy and mass of J/ψ and R is the nuclear force range. This approximation enables us to calculate the dissociation probability w with exponential accuracy regardless of the precise form of the J/ψ wave function. This is especially important since solutions of the relativistic two-body problem for quarkonium are not readily available.

It is natural to study quarkonium ionization in the comoving frame [12]. Quark energy ε_0 ($\varepsilon_0 < m$) in electromagnetic field can be written as

$$\varepsilon_0 = \sqrt{m^2 + (\boldsymbol{p} - e\boldsymbol{A})^2} + e\varphi = \sqrt{m^2 + (p_z + eBx)^2 + p_x^2 + p_y^2} - eEx. \tag{11}$$

In terms of ε_0, quarkonium binding energy is $\varepsilon_b = m - \varepsilon_0$. Ionization probability of quarkonium equals its tunneling probability through the potential barrier. The later is given by the transmission coefficient

$$w = e^{-2\int_0^{y_1} \sqrt{-p_y^2}\, dy} \equiv e^{-f}. \tag{12}$$

In the non-relativistic approximation one can also calculate the pre-exponential factor, which appears due to the deviation of the quark wave function from the quasi-classical approximation. The result of the calculation reads [12]:

$$\begin{aligned} \frac{f}{m^2} = {} & \frac{\sqrt{-\epsilon_0^2 + 1 + q^2}\,(\epsilon_0 E - qB)}{e(B^2 - E^2)} \\ & - \frac{(\epsilon_0 E - qB)^2 - (B^2 - E^2)(-\epsilon_0^2 + 1 + q^2)}{e(B^2 - E^2)^{3/2}} \\ & \times \ln\left\{ \frac{\epsilon_0 E - qB + \sqrt{(B^2 - E^2)(-\epsilon_0^2 + 1 + q^2)}}{\sqrt{(\epsilon_0 E - qB)^2 - (B^2 - E^2)(\epsilon_0^2 + 1 + q^2)}} \right\}, \end{aligned} \tag{13}$$

where $\epsilon_0 = \varepsilon_0/m$ and $q = p_z/m$.

For different q's function $w = e^{-f}$ gives the corresponding ionization probabilities. The largest probability corresponds to smallest f, which occurs at momentum q_m determined by equation [14]

$$\frac{\partial f(q_m)}{\partial q_m} = 0. \tag{14}$$

Using Eq. (13) we find [12]

$$\frac{\rho(\epsilon_0 - \rho q_m)}{1 - \rho^2} \ln\left\{ \frac{\epsilon_0 \rho - q_m + \sqrt{1 - \rho^2}\,\sqrt{-\epsilon_0^2 + 1 + q_m^2}}{\sqrt{(\epsilon_0 - \rho q_m)^2 - 1 + \rho^2}} \right\} = \frac{\sqrt{-\epsilon_0^2 + 1 + q_m^2}}{\sqrt{1 - \rho^2}}. \tag{15}$$

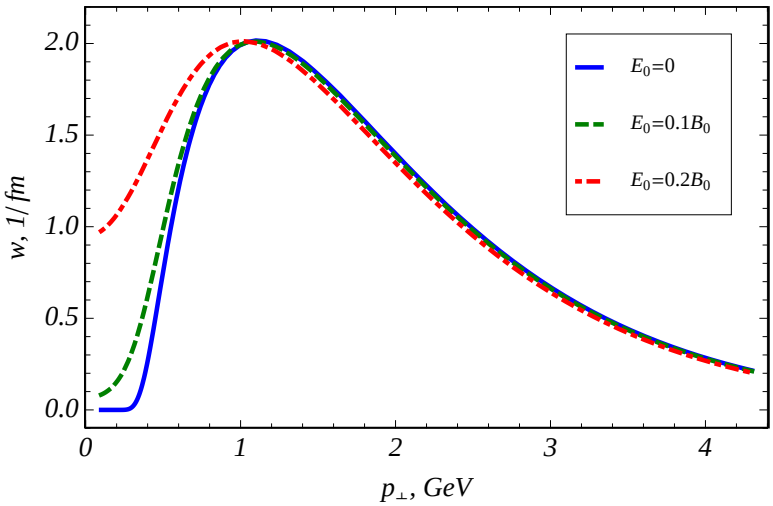

Figure 3: Dissociation rate of J/ψ at $eB_0 = 15m_\pi^2$, $\phi = \pi/2$ (in the reaction plane), $\eta = 0$ (midrapidity) as a function of J/ψ transverse momentum in the Lab frame $p_\perp$.

This is an implicit equation for the extremal momentum $q_m = q_m(\epsilon_0, \rho)$. Substituting q_m into Eq. (13) one obtains $f = f(\epsilon_0, \rho)$, which by means of Eq. (12) yields the ionization probability. The quasi-classical approximation that we employed in this section is valid inasmuch as $f(q_m) \gg 1$.

In the non-relativistic approximation we get a familiar result

$$f(q_m) = \frac{2m^2(2\epsilon_b)^{3/2}}{3eE}\, g(\gamma), \tag{16}$$

where $g(\gamma)$ is the Keldysh function

$$g(\gamma) = \frac{3\tau_0}{2\gamma}\left[1 - \frac{1}{\gamma}\left(\frac{\tau_0^2}{\gamma^2} - 1\right)^{1/2}\right], \tag{17}$$

and $\gamma = \frac{\sqrt{2\epsilon_b}}{\rho}$ is the adiabaticity parameter.

It is shown in Ref. [12] that the non-relativistic limit provides a very good approximation to the dissociation rate. It also allows one to calculate the pre-exponential factor [14–16]. The final result is depicted in Fig. 3 [13]. We also show the dissociation rate of J/ψ for several values of the electric field $\boldsymbol{E}_0$ possibly induced by the Chiral Magnetic Effect [6]. Note, that typical size of the medium traversed by a J/ψ in magnetic field can be estimated very conservatively as a few fm. Therefore, $w \sim 0.3$–0.5 fm^{-1} corresponds to complete destruction of J/ψ's. This means that in the magnetic field of strength $eB_0 \sim 15m_\pi^2$ all J/ψ's with $p_\perp \gtrsim 0.5$ GeV are destroyed independently of the strength of E_0.

Angular distribution of J/ψ's was discussed in detail in Ref. [13]. In the absence of electric field $\boldsymbol{E}_0$, the dissociation probability peaks in the direction perpendicular to the direction of magnetic field $\boldsymbol{B}_0$, i. e. in the reaction plane. Dissociation rate vanishes in the $\boldsymbol{B}_0$ direction. The shape of the azimuthal distribution strongly depends on quarkonium velocity: while at low V the strongest dissociation is in the direction of the reaction plane, at higher V the maximum shifts towards small angles around the $\boldsymbol{B}_0$ direction.

4 Synchrotron radiation

As a second example, consider electromagnetic radiation by quark and anti-quarks in plasma. QGP is transparent to the emitted electromagnetic radiation because its absorption coefficient is suppressed by α^2. Electromagnetic radiation by quarks and antiquarks of QGP moving in external magnetic field originates from two sources: (i) synchrotron radiation and (ii) quark and antiquark annihilation. It is argued in Ref. [17] that contribution of annihilation channel is negligible, hence we focus on synchrotron radiation. In strong magnetic field it is essential to account for quantization of fermion spectra. Indeed, spacing between the Landau levels is of the order eB/ε (ε being quark energy), while their thermal width is of the order T. Spectrum quantization is negligible only if $eB/\varepsilon \ll T$ which is barely the case at RHIC and certainly not the case at LHC (at least during the first few fm's of the evolution).

Synchrotron radiation is a process of photon γ radiation by a fermion f with electric charge $e_f = z_f e$ in external magnetic field B: $f(e_f, j, p) \to f(e_f, k, q) + \gamma(\boldsymbol{k})$, where $\boldsymbol{k}$ is the photon momentum, p, q are the momentum components along the magnetic field direction and indices j, $k = 0, 1, 2, ...$ label the discrete Landau levels in the reaction plane. The Landau levels are given by

$$\varepsilon_j = \sqrt{m^2 + p^2 + 2je_fB}, \qquad \varepsilon_k = \sqrt{m^2 + q^2 + 2ke_fB}. \tag{18}$$

In constant magnetic field only momentum component along the field direction is conserved. Thus, the conservation laws for synchrotron radiation read

$$\varepsilon_j = \omega + \varepsilon_k, \qquad p = q + \omega\cos\theta, \tag{19}$$

where ω is the photon energy and θ is the photon emission angle with respect to the magnetic field. Spectral intensity of angular distribution of synchrotron radiation by a fermion in the j'th Landau state is given by [18]

$$\frac{dI^j}{d\omega d\Omega} = \sum_f \frac{z_f^2\alpha}{\pi}\,\omega^2 \sum_{k=0}^{j} \Gamma_{jk}\left\{|\mathcal{M}_\perp|^2 + |\mathcal{M}_\parallel|^2\right\}\delta(\omega - \varepsilon_j + \varepsilon_k), \tag{20}$$

where $\Gamma_{jk} = (1+\delta_{j0})(1+\delta_{k0})$ accounts for the double degeneration of all Landau levels except the ground one. The squares of matrix elements $\mathcal{M}$, which appear in Eq. (20) can be found in Ref. [18] (our notations follow Ref. [19]).

In the context of heavy-ion collisions the relevant observable is the differential photon spectrum. For ideal plasma in equilibrium each quark flavor gives the following contribution to the photon spectrum:

$$\frac{dN^{\rm synch}}{dtd\Omega d\omega} = \sum_f \int_{-\infty}^{\infty} dp\,\frac{e_fB(2N_c)V}{2\pi^2} \sum_{j=0}^{\infty}\sum_{k=0}^{j} \frac{dI^j}{\omega d\omega d\Omega}\,(2-\delta_{j,0})\,f(\varepsilon_j)\,[1-f(\varepsilon_k)], \tag{21}$$

where $2N_c$ accounts for quarks and antiquarks each of N_c possible colors, and $(2-\delta_{j,0})$ sums over the initial quark spin. Index f indicates different quark flavors. V stands for the plasma volume. $f(\varepsilon)$ is a statistical factor. The δ-function appearing in Eq. (20) yields a constraint on the quark's momentum

$$p_\pm^* = \Big\{\cos\theta\,(m_j^2 - m_k^2 + \omega^2\sin^2\theta) \\ \pm\sqrt{\left[(m_j+m_k)^2 - \omega^2\sin^2\theta\right]\left[(m_j-m_k)^2 - \omega^2\sin^2\theta\right]}\Big\}\Big/(2\omega\sin^2\theta), \tag{22}$$

where $m_j^2 = m^2 + 2je_fB$, $m_k^2 = m^2 + 2ke_fB$. Inspection of Eq. (22) reveals that this equation has a real solution only in two cases

$$\text{(i) } m_j - m_k \geq \omega\sin\theta, \qquad \text{or} \qquad \text{(ii) } m_j + m_k \leq \omega\sin\theta. \tag{23}$$

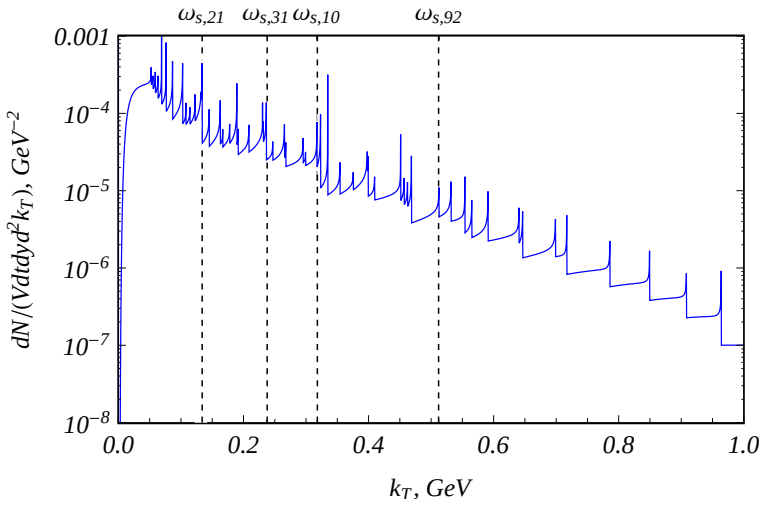

Figure 4: Spectrum of synchrotron radiation by u quarks at $eB = m_\pi^2$, $y = 0$, $\phi = \pi/3$: contribution of 10 lowest Landau levels $j \leq 10$; several cutoff frequencies are indicated. Adopted from Ref. [17].

The first case is relevant for the synchrotron radiation while the second one for the one-photon pair annihilation. Accordingly, allowed photon energies in the $j \to k$ transition satisfy

$$\omega \leq \omega_{s,jk} \equiv \frac{m_j - m_k}{\sin\theta} = \frac{\sqrt{m^2 + 2je_fB} - \sqrt{m^2 + 2ke_fB}}{\sin\theta}\,. \tag{24}$$

No synchrotron radiation is possible for $\omega > \omega_{s,jk}$ (see Fig. 4). In particular, when $j = k$, $\omega_{s,jk} = 0$, i. e. no photon is emitted. The reason is clearly seen in the frame where $p = 0$: since $\varepsilon_j \geq \varepsilon_k$, constraints (18) and (19) hold only if $\omega = 0$.

Substitution of (20) into Eq. (21) yields the spectral distribution of the synchrotron radiation rate per unit volume

$$\frac{dN^{\rm synch}}{Vdtd\Omega d\omega} = \sum_f \frac{2N_c z_f^2 \alpha}{\pi^3}\, e_f B \sum_{j=0}^{\infty}\sum_{k=0}^{j} \omega(1+\delta_{k0})\,\vartheta(\omega_{s,ij}-\omega) \int dp \sum_{\pm} \frac{\delta(p - p_\pm^*)}{\left|\frac{p}{\varepsilon_j} - \frac{q}{\varepsilon_k}\right|}$$
$$\times \left\{|\mathcal{M}_\perp|^2 + |\mathcal{M}_\parallel|^2\right\} f(\varepsilon_j)[1 - f(\varepsilon_k)], \tag{25}$$

where ϑ is the step-function.

The natural variables to study the synchrotron radiation are the photon energy ω and its emission angle θ with respect to the magnetic field. However, in high energy physics particle spectra are traditionally presented in terms of rapidity y (which for photons is equivalent to pseudo-rapidity) and transverse momentum $k_\perp$. $k_\perp$ is a projection of three-momentum $\boldsymbol{k}$ onto the transverse plane. These variables are not convenient to study electromagnetic processes in external magnetic field. In particular, they conceal the azimuthal symmetry with respect to the magnetic field direction. The change of variables is performed using formulas

$$\omega = k_\perp \cosh y, \qquad \cos\theta = \frac{\sin\phi}{\cosh y}\,. \tag{26}$$

Because $dy = dk_z/\omega$ the photon multiplicity in a unit volume per unit time reads

$$\frac{dN^{\rm synch}}{dV\,dt\,d^2k_\perp dy} = \omega\frac{dN^{\rm synch}}{dV\,dt\,d^3k} = \frac{dN^{\rm synch}}{dV\,dt\,\omega d\omega d\Omega} \tag{27}$$

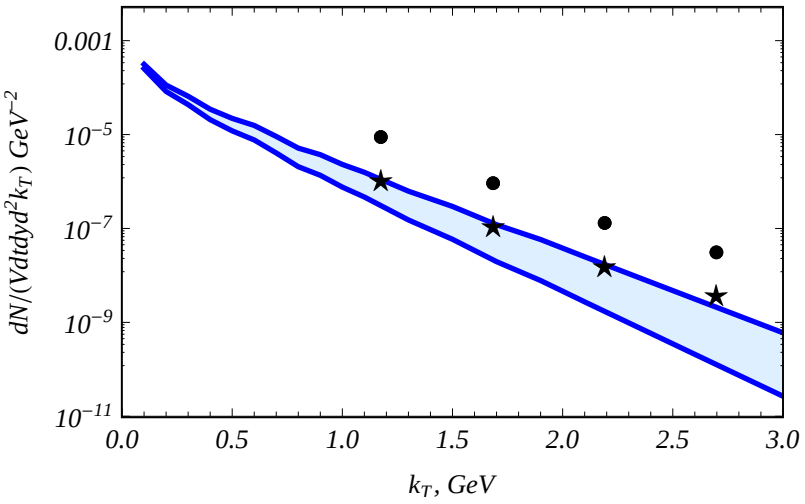

Figure 5: Azimuthal average of the synchrotron radiation spectrum of u, d, s quarks and their corresponding antiquarks compared to the experimental data from Ref. [20] divided by $Vt = 25\pi$ fm^4 (dots) and $Vt = 9 \times 25\pi$ fm^4 (stars); $eB = m_\pi^2$, $y = 0$. Lower line: $T = 200$ MeV, upper line: $T = 250$ MeV. Adopted from Ref. [17].

Figure 4 displays the spectrum of synchrotron radiation by u quarks as a function of $k_\perp$ at fixed ϕ [17]. At midrapidity $y = 0$, Eq. (26) implies that $k_\perp = \omega$. Contribution of d and s quarks is qualitatively similar. At $eB \gg m^2$, quark masses do not affect the spectrum much. The main difference stems from the difference in electric charge. In Fig. 4 only the contributions of the first ten Landau levels are displayed. The cutoff frequencies $\omega_{s,jk}$ can be clearly seen and some of them are indicated on the plot for convenience.

In order to compare the photon spectrum produced by synchrotron radiation to the photon spectrum measured in heavy-ion collisions, the u, d and s quarks contributions must be summed up. Furthermore, the experimental data from Ref. [20] should be divided by Vt, where t is the magnetic field relaxation time. The volume of the plasma can be estimated as $V = \pi R^2 t$ with $R \approx 5$ fm being the nuclear radius. The results are plotted in Fig. 5. It is seen that synchrotron radiation gives a significant contribution to the photon production in heavy-ion collisions at low k_T's. This is the region where conventional models of photon production fail to explain the experimental data.

5 Summary

High intensity and long life-time of electromagnetic field produced in relativistic heavy ion collisions indicate its phenomenological significance. In this presentation I discussed only two examples. It is clear however that the electromagnetic field changes the very structure of quark-gluon plasma and leaves hardly any observable unaffected. The ongoing experimental programs at RHIC and LHC can shed more light on the properties of hot nuclear matter in intense electromagnetic field.

References

[1] L. D. Landau, Izv. Akad. Nauk Ser. Fiz. **17**, 51 (1953).

[2] S. Z. Belenkij and L. D. Landau, Nuovo Cim. Suppl. **3S10**, 15 (1956) [Usp. Fiz. Nauk **56**, 309 (1955)].

[3] P. F. Kolb and U. W. Heinz, in *Quark gluon plasma 3*, eds. R. C. Hwa and X.-N. Wang. World Scientific, Singapore, 2004, p. 634, nucl-th/0305084 (2003).

[4] K. Tuchin, arXiv:1305.5806 [hep-ph] (2013).

[5] K. Tuchin, Adv. High Energy Phys. **2013**, 490495 (2013), arXiv:1301.0099 [hep-ph] (2013).

[6] D. E. Kharzeev, L. D. McLerran and H. J. Warringa, Nucl. Phys. A **803**, 227 (2008).

[7] K. Tuchin, Phys. Rev. C **82**, 034904 (2010); Erratum: *ibid.* **83**, 039903 (2011).

[8] H. T. Ding, A. Francis, O. Kaczmarek, F. Karsch, E. Laermann and W. Soeldner, arXiv:1012.4963 [hep-lat] (2010).

[9] G. Aarts, C. Allton, J. Foley, S. Hands and S. Kim, Phys. Rev. Lett. **99**, 022002 (2007), arXiv:hep-lat/0703008 (2007).

[10] A. Amato, G. Aarts, C. Allton, P. Giudice, S. Hands and J. -I. Skullerud, arXiv:1307.6763 [hep-lat] (2013).

[11] B. Machet and M. I. Vysotsky, Phys. Rev. D **83**, 025022 (2011), arXiv:1011.1762 [hep-ph] (2010).

[12] K. Marasinghe and K. Tuchin, Phys. Rev. C **84**, 044908 (2011), arXiv:1103.1329 [hep-ph] (2011).

[13] K. Tuchin, Phys. Lett. B **705**, 482 (2011), arXiv:1105.5360 [nucl-th] (2011).

[14] V. S. Popov, B. M. Karnakov and V. D. Mur, Phys. Lett. A **250**, 20 (1998).

[15] V. S. Popov, B. M. Karnakov and V. D. Mur, Phys. Lett. A **229**, 306 (1997).

[16] V. S. Popov, B. M. Karnakov and V. D. Mur, JETP **86**, 860 (1998).

[17] K. Tuchin, Phys. Rev. C **87**, 024912 (2013), arXiv:1206.0485 [hep-ph] (2012).

[18] A. A. Sokolov and I. M. Ternov, *Synchrotron radiation*. Pergamon Press, Oxford, 1968.

[19] M. G. Baring, Mon. Not. R. Ast. Soc. **235**, 57, (1988).

[20] A. Adare *et al.* (PHENIX Collaboration), Phys. Rev. Lett. **104**, 132301 (2010).